2018

Eccentrically Loaded FRP Confined Concrete with Different Wrapping Schemes

Weiqiang Wang
University of Technology Sydney, ww674@uowmail.edu.au

Patrick R. Martin
University of Wollongong, pm843@uowmail.edu.au

M Neaz Sheikh
University of Wollongong, msheikh@uow.edu.au

Muhammad N. S Hadi
University of Wollongong, mhadi@uow.edu.au

Eccentrically Loaded FRP Confined Concrete with Different Wrapping Schemes

Abstract

This study presents the results of an experimental program on the comparative performance of fiber-reinforced polymer (FRP) confined concrete specimens with different wrapping schemes. A total of 32 specimens in four groups were cast and tested under concentric and eccentric axial loads. All specimens were wrapped with the same amount of FRP but with different wrapping schemes, including full wrapping, partial wrapping, and nonuniform wrapping. Specimens in the first group were fully wrapped (Group F). Specimens in the second group were partially wrapped with 30 mm FRP strip spacing (Group P30). Specimens in the third group were partially wrapped with 60 mm FRP strip spacing (Group P60). Specimens in the fourth group were nonuniformly wrapped with a combination of full and partial wrapping (Group FP). Two similar specimens in each group were tested under concentric, 15 mm eccentric, 25 mm eccentric, and 40 mm eccentric axial loads. The test results indicate that fully wrapped specimens outperformed other groups of specimens under both concentric and eccentric axial loads, which were followed by nonuniformly and partially wrapped specimens. With the increase in axial load eccentricity, the performance in all groups significantly decreased. Moreover, with the increase in axial load eccentricity, the failure mode changed from FRP rupture at the compression side to extensive concrete cracking at the tension side. Equations were developed to predict the compressive strength of FRP confined concrete with different wrapping schemes. Experimental and analytical interaction (P-M) diagrams were also constructed to investigate the axial and flexural behavior of different groups of specimens.

Disciplines

Engineering | Science and Technology Studies

Publication Details

Wang, W., Martin, P. R., Sheikh, M. Neaz. & Hadi, M. N. S. (2018). Eccentrically Loaded FRP Confined Concrete with Different Wrapping Schemes. Journal of Composites for Construction, 22 (6), 04018056-1-04018056-15.

Eccentrically Loaded FRP Confined Concrete with Different Wrapping Schemes

Weiqiang Wang, A.M.ASCE[1]; Patrick R. Martin[2]; M. Neaz Sheikh[3], and Muhammad N.S. Hadi, F.ASCE[4]

Abstract: This study presents the results of an experimental program on the comparative performance of fiber reinforced polymer (FRP) confined concrete specimens with different wrapping schemes. A total of 32 specimens in four groups were cast and tested under concentric and eccentric axial loads. All specimens were wrapped with the same amount of FRP but with different wrapping schemes, including full wrapping, partial wrapping, and non-uniform wrapping. Specimens in the first group were fully wrapped (Group F). Specimens in the second group were partially wrapped with 30 mm FRP strip spacing (Group P30). Specimens in the third group were partially wrapped with 60 mm FRP strip spacing (Group P60). Specimens in the fourth group were non-uniformly wrapped with a combination of full and partial wrapping (Group FP). Two similar specimens in each group were tested under concentric, 15 mm eccentric, 25 mm eccentric, and 40 mm eccentric axial loads. The test results indicate that fully wrapped specimens outperformed other groups of specimens under both concentric and eccentric axial loads, which were followed by non-uniformly and partially wrapped specimens. With the increase in axial load eccentricity, the performance in all groups significantly decreased. Moreover, with the increase in axial load eccentricity, the failure mode changed from FRP rupture at the compression side to extensive concrete cracking at the tension side. Equations were developed to predict the compressive strength of FRP confined concrete with different wrapping schemes. Experimental and analytical interaction (*P-M*) diagrams were also constructed to investigate the axial and flexural behavior of different groups of specimens.

CE Database subject headings: FRP; Partial; Non-uniform; Concrete; Eccentricity; Interaction diagram.

---

[1] Research associate, Centre for Built Infrastructure Research, School of Civil and Environmental Engineering, University of Technology Sydney, NSW 2007, Australia. E-mail: Weiqiang.Wang@uts.edu.au, ww674@uowmail.edu.au
[2] Former undergraduate student, School of Civil, Mining and Environmental Engineering, University of Wollongong, Wollongong NSW 2522 Australia. E-mail: pm843@uowmail.edu.au
[3] Associate professor, School of Civil, Mining and Environmental Engineering, University of Wollongong, Wollongong NSW 2522 Australia. E-mail: msheikh@uow.edu.au
[4] Associate professor, School of Civil, Mining and Environmental Engineering, University of Wollongong, Wollongong NSW 2522, Australia (corresponding author). E-mail: mhadi@uow.edu.au

Introduction

Fiber reinforced polymer (FRP) has been extensively investigated to provide confinement to concrete due to the advantages of high strength and stiffness to weight ratio as well as superior corrosion resistance. A large number of experimental and analytical studies were conducted in the literature to understand and model the compressive behavior of FRP confined concrete. It was proved that FRP confinement can significantly enhance the performance of concrete under compressive loads (Lam and Teng 2003a, b; Hadi 2006a, b; Hadi et al. 2015; Wang et al. 2016; Wang et al. 2017).

Even though a considerable number of studies were conducted on fully FRP wrapped concrete, only a few studies focused on partially FRP wrapped concrete (Barros and Ferreira 2008; Park et al. 2008; Campione et al. 2015; Pham et al. 2015; Triantafyllou et al. 2015; Saljoughian and Mostofinejad 2016). Partial FRP wrapping requires less FRP materials and can be applied easier and faster than full wrapping (Pham et al. 2015). Moreover, for existing reinforced concrete (RC) columns confined with sparse steel ties, the compressive performance of existing RC columns is expected to be improved by partial FRP wrapping in between the sparse steel ties, as the local buckling of longitudinal steel bars can be effectively constrained by the partial FRP wrapping (Triantafyllou et al. 2015). Furthermore, for existing deteriorated RC columns, partial FRP wrapping onto the deteriorated part of the RC columns can significantly increase the strength and ductility of the columns without consuming excessive FRP materials which otherwise would be required for the full wrapping of the RC columns (Wei et al. 2009). Few studies also investigated the use of composite taps and ropes as the confinement materials for concrete in the form of full or partial wrapping (Rousakis 2014, 2016).

Several research studies investigated the behavior of partially FRP wrapped concrete under axial compressive load (Matthys et al. 2005; Barros and Ferreira 2008; Triantafyllou et al. 2014; Pham et al. 2015). Among these studies, Barros and Ferreira (2008) systematically investigated the confinement efficiency of partially FRP wrapped plain and RC column specimens. It was reported that a significant increase in the load carrying capacity and deformation capacity can be obtained by reducing the FRP strip spacing and reducing the unconfined concrete strength, or increasing the confinement stiffness of FRP jacket (Barros and Ferreira 2008). Pham et al. (2015) investigated the axial compressive behavior of FRP wrapped concrete with different FRP wrapping schemes. In Pham et al. (2015), a non-uniform FRP wrapping scheme with a combination of full and partial FRP wrapping was proposed. It was reported that higher axial compressive strength and axial strain, in comparison with full FRP wrapping scheme, could be obtained by non-uniform FRP wrapping. Moreover, an equation was proposed to predict the compressive strength of partially FRP wrapped concrete.

Concrete columns are often subjected to the combined axial and flexural loads in practical situations. Several studies investigated the behavior of fully FRP wrapped concrete under eccentric loads. It was concluded that the strain gradient effect caused a non-uniform confining pressure which reduced the efficiency of the FRP confinement under eccentric loads (Parvin and Wang 2001; Hadi 2006 a,b; Wu and Jiang 2013). Even though partial FRP wrapping is considered to be promising in some particular applications, studies on partially FRP wrapped concrete under eccentric load are limited. Moreover, none of the previous studies provided information on non-uniformly FRP wrapped concrete under eccentric load. This study investigates the behavior of FRP confined plain concrete specimens with different wrapping schemes under concentric and eccentric axial loads. An experimental program was conducted to

investigate the comparative performance of fully, partially, and non-uniformly FRP wrapped concrete under concentric and eccentric axial loads (eccentricity of 15 mm, 25 mm, and 40 mm). The failure modes, axial load-axial deformation behaviors, ductility capacity, and axial load-bending moment interactions *(P-M)* of the specimens were investigated. Moreover, an analytical procedure was developed to predict the axial and flexural behaviors of the tested specimens with the aim to better understand the ultimate capacities of all groups of specimens.

Experimental Program

Design of Experiments

A total of 32 concrete specimens were cast and tested under concentric and eccentric axial loads. All the specimens were 150 mm in diameter and 300 mm in height. Four groups of specimens, with 8 specimens in each group, were divided based on the FRP wrapping schemes. All groups of specimens were wrapped with same amount of FRP but following different wrapping schemes. The aim was to investigate the influence of different wrapping schemes on the behavior of FRP wrapped concrete under concentric and eccentric axial loads. Specimens in the first group were fully wrapped with two layers of carbon fiber reinforced polymer (CFRP), as shown in Fig. 1(a). Specimens in the second group were partially wrapped with four layers of 30 mm wide FRP strips, and the spacing between neighboring FRP strips was 30 mm, as shown in Fig. 1(b). Specimens in the third group were partially wrapped with six layers of 30 mm wide FRP strips, while the spacing between neighboring FRP strips was 60 mm, as shown in Fig. 1(c). Specimens in the fourth group were non-uniformly wrapped, as shown in Fig. 1(d). For the fourth group of specimens, at first, the specimens were fully wrapped with one layer of FRP. Afterwards, two layers of 30 mm wide FRP strips were wrapped onto the first layer of FRP with 30 mm spacing between neighboring FRP strips. It is noted that the amount of FRP for Group P30 and FP

104 specimens were slightly different from those of Group F and P60 specimens (Fig. 1). This slight
105 difference was mainly due to the length of the specimen, which made it difficult to maintain
106 exactly the same amount of FRP. However, it is believed that this slight difference might not
107 affect the results, since all the specimens were expected to fail in the mid-height region. In the
108 mid-height region, the wrapping configurations were different, but the amount of FRP were
109 exactly the same.
110 For specimens in each group, two identical specimens were tested under the same load
111 conditions to ensure representative test results. Axial load eccentricities of 0, 15, 25, and 40 mm
112 were adopted in this study, where zero eccentricity corresponds to concentric axial load. Table 1
113 lists the detailed test matrix. The specimens have been labelled as: (a) "F", "P30", "P60", and
114 "FP" represent fully wrapped, partially wrapped with 30 mm FRP strip spacing, partially
115 wrapped with 60 mm FRP strip spacing, and non-uniformly wrapped specimens, respectively; (b)
116 "E" and the number afterwards indicate load eccentricity (0 indicates concentric axial load; 15
117 indicates eccentric axial load with 15 mm eccentricity; 25 indicates eccentric axial load with 25
118 mm eccentricity; and 40 indicates eccentric axial load with 40 mm eccentricity); and (c) "1" or
119 "2" indicates the order of the two identical specimens tested under the same axial load conditions.
120
121 ***Specimen Preparation and Material Properties Test***
122 The CFRP sheet used in this study was supplied by Nanjing Hitech Composites CO., LTD
123 (2016). The original width of CFRP sheet was 100 mm and the thickness was 0.167 mm per
124 layer. For fully wrapped specimens, the 100 mm wide CFRP sheet was wrapped onto the top,
125 middle, and bottom parts of the specimens. Therefore, there was no overlap between the parts, as
126 each part was 100 mm. In order to obtain the required width of CFRP strip for partially wrapped

specimens, each CFRP strip was precisely cut from the original CFRP sheet using a pair of scissors.

Normal strength concrete with a design compressive strength of 32 MPa was used for casting the specimens. The concrete was supplied by a local concrete provider with a maximum aggregate size of 10 mm. After 28 days of standard curing, the concrete specimens were wrapped with CFRP. A mixture of epoxy resin and hardener at a ratio of 5:1 was used as an adhesive. Preparations of fully and partially FRP wrapped specimens were similar: before the first layer of CFRP was wrapped, the adhesive was evenly spread onto the surface of the specimen and then CFRP was wrapped onto the specimen surface with the fibers oriented in the hoop direction. Immediately after the first layer was wrapped, the adhesive was evenly spread onto the surface of the first layer of CFRP and the second layer was continuously wrapped. The remaining layers of CFRP were wrapped in a similar manner. An overlap of 100 mm was ensured in the last layer of CFRP strips. While for non-uniformly FRP wrapped specimens, the specimens were left for a while until the adhesive was hardened after the one layer full wrapping was conducted. Afterwards, the remaining CFRP strips were wrapped.

Compression tests at 28 days showed that the average compressive strength of the concrete was 37.7 MPa. The tensile properties of CFRP were tested according to ASTM D7565 (ASTM 2010). Five CFRP coupons with 25 mm width and 250 mm length were prepared and tested. For each coupon, three layers of CFRP were glued together using epoxy resin. The coupons were capped at both ends by aluminum plates. Detailed description of the test can be found in Wang et al.

149 (2016). The average nominal thickness of the coupons was 1.18 mm, and the average tensile
150 strength of CFRP was 1674 MPa with an average ultimate strain of 0.016.
151
152 ***Instrumentation***
153 The Denison 5,000 kN compression testing machine was used for testing all the specimens. For
154 concentrically and eccentrically loaded specimens, the specimen ends were capped with high-
155 strength plaster to ensure a uniform load distribution. In order to apply eccentric axial load onto
156 the specimens, a set of loading heads were used (Figs. 2 (a) and (b)). Axial deformations of the
157 specimens were measured using two Linear Variable Differential Transducers (LVDTs), which
158 were mounted at the opposite corners between the loading plate and the supporting plate of the
159 Denison testing machine. Therefore, the height of the specimens used to obtain the axial
160 deformations from LVDTs was 300 mm. In order to measure the lateral deflections for the
161 eccentrically loaded specimens, a laser triangulation was used. The laser triangulation was
162 manufactured by Bestech Australia Pty Ltd. (2018). The laser triangulation was positioned onto
163 the bottom loading plate by using a magnetic base and was set up at the mid-height of the
164 specimen, as shown in Fig. 2 (c). For the specimens tested under 15 and 25 mm eccentric axial
165 loads, the laser triangulation was positioned on the tension side. However, as few specimens
166 failed in an explosive manner, the laser triangulation was moved to the compression side for the
167 specimens tested under 40 mm eccentric axial load to prevent the probable damage of the laser
168 triangulation. All the tests were conducted as deflection controlled at a rate of 0.5 mm/min. The
169 readings of the load and LVDTs were taken using a data logging system and were subsequently
170 saved in a control computer.
171

Experimental Results and Analysis

Specimens under Concentric Axial Load

The failure modes of concentrically loaded specimens are presented in Fig. 3. All concentrically loaded specimens failed due to the brittle rupture of CFRP. For partially FRP wrapped concrete specimens, small cracks were observed on the surface of non-wrapped concrete during the loading. As the load increased, the non-wrapped concrete began to crush and spall off. The spalling of non-wrapped concrete was more severe for specimens with 60 mm strip spacing. The spalling of non-wrapped concrete was then followed by the rupture of the CFRP strips around the mid height of the specimens. For Specimens FP-E0, the one layer CFRP ruptured first, resulting in a small and sudden drop in the axial load. Afterwards, the axial load began to increase again until the three layers CFRP at the mid height of specimens ruptured, causing a fatal failure.

The test results for concentrically loaded specimens are presented in Table 2. The axial load at the elastic limit P_1 and the corresponding axial deformation Δ_1, the peak axial load P_2 and the corresponding axial deformation Δ_2, the ductility μ, as well as the failure mode, are presented in Table 2. In this study, the definition on the axial load at the elastic limit P_1 in Pessiki and Pieroni (1997) was used for specimens that exhibited strain softening response, as shown in Figs. 4 (a) and (b). However, this definition was unable to accurately determine P_1 for specimens which exhibited strain hardening response (Dong et al. 2015). In this case, the definition given by Dong et al. (2015) was adopted, as shown in Fig. 4 (c).

194 The peak axial loads of Specimens F-E0 were the highest among the concentrically loaded
195 specimens, which were on average 68% higher than those of the Specimens P60-E0. Specimens
196 FP-E0 achieved peak axial loads that were on average 52% higher than those achieved by
197 Specimens P60-E0. An average of 46% increase in the peak axial loads compared to Specimens
198 P60-E0 was achieved by Specimens P30-E0. Fig. 5 shows the axial load-axial deformation
199 behavior of concentrically loaded specimens. Since the lateral deflections for concentrically
200 loaded specimens were very small, they were not recorded by using the laser triangulation setup.
201 Moreover, for comparisons, the axial load-axial deformation behavior of plain concrete
202 specimens was also presented. All specimens exhibited similar behavior at the initial stage, while
203 the slope of the second branch varied significantly between different groups of specimens. For
204 plain concrete specimens (P-E0-1, 2), the axial load decreased significantly after the peak axial
205 load and finally lost all the strength with a small axial deformation. Typical bilinear curves for
206 concentrically loaded FRP confined concrete specimens. The slope of the second linear branch
207 for Specimens F-E0 and FP-E0 was almost identical and the highest, followed by those of
208 Specimens P30-E0 and Specimens P60-E0. It is noted that even though extensive concrete
209 cracking occurred for Specimens P30-E0 and P60-E0, the FRP strips prevented the axial load
210 from dropping and ensured continuous increases of the axial load (Campione 2015; Rousakis
211 2014, 2016). On the other hand, the FRP confinement efficiency was highly dependent on the
212 strip spacing: the less the strip spacing, the higher the confinement efficiency. Even though the
213 load-deformation behavior of Specimens F-F0 was quite similar to the load-deformation
214 behavior of Specimens FP-E0, Specimens FP-E0 failed earlier than Specimens F-E0. A slight
215 drop in the axial load can be observed for Specimens FP-E0, which was due to the rupture of one
216 layer CFRP. Afterwards, the axial load continued to increase slightly until the rupture of three

217 layers CFRP. For non-uniformly FRP confined concrete specimens, the rupture of one layer
218 CFRP can be used as a suitable indication before the final rupture of the specimens. Moreover,
219 even though Specimens P60-E0 achieved the lowest peak axial loads, the axial deformation was
220 the highest, which was mainly because significant strain localization occurred within the non-
221 wrapped region (Wei and Wu 2016).
222
223 ***Specimens under 15 mm Eccentric Axial Load***
224 The failure modes of specimens under 15 mm eccentric axial load are presented in Fig. 6.
225 Specimens F-E15, FP-E15, and P30-E15 failed by the CFRP rupture at the mid height of the
226 specimens on the compression side. For Specimens FP-E15, the one layer CFRP above and
227 below the mid height of the compression side ruptured first. This was followed by a continuous
228 axial load increase until the rupture of three layers of CFRP at the mid height of the compression
229 side. For Specimens P30-E15, tension cracks occurred within the non-wrapped concrete at the
230 mid height of the tension side. Afterwards, the tension cracks propagated approximately half way
231 through the specimen until the rupture of CFRP strips. The CFRP rupture for Specimen P30-
232 E15-1 was explosive, resulting in the specimen breaking into two halves. The failure of
233 Specimens P60-E15 was due to the propagation of the tension crack from the tension side to the
234 compression side. When the tension crack developed to the compression side, the specimens
235 failed and no CFRP rupture was observed for Specimens P60-E15.
236
237 The test results for specimens under 15 mm eccentric axial load are presented in Table 3. The
238 lowest peak axial loads were carried by Specimens P60-E15. Specimens F-E15 achieved the
239 greatest peak axial loads, which were on average 103% higher than those carried by Specimens

240 P60-E15. The peak axial loads of Specimens FP-E15 and P30-E15 were on average 75% and
241 47%, respectively, greater than the peak axial loads of Specimens P60-E15. Fig. 7 shows the
242 axial load-axial deformation behavior of Specimens F-E15, FP-E15, P30-E15, and P60-E15.
243 Specimens F-E15, FP-E15, and P30-E15 experienced strain hardening responses after the initial
244 parabolic ascending branches, while strain softening responses were observed in Specimens P60-
245 E15 due to insufficient confinement provided by the sparse CFRP strips. Also, the spalling of
246 non-wrapped concrete may have further resulted in the performance deterioration of partially
247 FRP confined specimens. Even though the peak axial loads of Specimens P30-E15 were
248 significantly less than the peak axial loads of Specimens F-E15 and FP-E15, the deformation
249 capacities of Specimens P30-E15 were even higher, which suggested that the strain localization
250 within non-wrapped region still existed for partially wrapped concrete under small load
251 eccentricities. Moreover, since the failures of Specimens P60-E15 were caused by extensive
252 concrete cracking on the tension side, the ultimate condition was defined when the axial load
253 dropped by 15% of the peak axial load. The corresponding lateral deflections at the ultimate
254 conditions were 9.9 and 9.3 mm, respectively, which were higher than those of other groups of
255 specimens (Table 3). Therefore, the gradual failure for Specimens P60-E15 resulted in a pseudo-
256 ductile behavior compared to other specimens.
257
258 ***Specimens under 25 mm Eccentric Axial Load***
259 The failure modes of specimens under 25 mm eccentric axial load are presented in Fig. 8.
260 Specimens F-E25 failed by CFRP rupture at the mid height of the compression side. Specimens
261 P30-E25 failed by a combination of CFRP rupture and concrete tension cracking failure. For
262 Specimens P30-E25, the non-wrapped concrete on the compression side crushed and two

263 horizontal tension cracks appeared above and below the middle CFRP strip on the tension side.
264 The horizontal tension cracks then started to propagate towards the compression side, which
265 resulted in a gradual decrease in axial load. Almost simultaneously, the CFRP strip at the mid
266 height ruptured and the horizontal tension cracks reached the compression side. Specimens P60-
267 E25 failed due to the propagation of horizontal tension crack initiated at the tension side. Failure
268 occurred when the horizontal crack propagated to the compression side, and no CFRP rupture
269 was observed. Specimens FP-E25 failed by the CFRP rupture on the compression side. The one
270 layer CFRP around the mid height ruptured first, which was followed by the rupture of three
271 layers of CFRP on the compression side.
272
273 The test results of specimens under 25 mm eccentric axial load are presented in Table 3.
274 Specimens P60-E25 carried the lowest peak axial loads. Considering Specimens P60-E25 as a
275 basis of comparison, Specimens F-E25 carried the largest peak axial loads, which were on
276 average 70% higher. The peak axial loads carried by Specimens FP-E25 and P30-E25 were on
277 average 48% and 22% greater than the peak axial loads carried by Specimens P60-E25,
278 respectively. The axial load-axial deformation behavior of Specimens F-E25, FP-E25, P30-E25,
279 and P60-E25 are shown in Fig. 9. It was apparent that the post-peak behavior of the specimens
280 varied between different groups of specimens. Specimens F-E25 and FP-E25 presented post-
281 peak ascending branches, whereas Specimens P60-E25 presented post-peak descending branches.
282 The post-peak branches of Specimens P30-E25 were initially ascending before reaching the peak
283 axial load at which the curves transitioned from ascending to descending. It should be noted that
284 for Specimens P30, the CFRP rupture did not occur until the occurrence of descending branch,

285 which indicated that the confinement provided by the FRP strips was not maximum at peak axial
286 load.
287
288 ***Specimens under 40 mm Eccentric Axial Load***
289 The failure modes of specimens under 40 mm eccentric load are presented in Fig. 10. All
290 specimens experienced extensive concrete tension cracks from the tension side to the
291 compression side. For Specimens P60-E40, the propagation of the horizontal tension cracks
292 occurred relatively quickly compared to the other groups of specimens, which resulted in a much
293 quicker failure. For Specimens FP-E40, the tension cracks initiated at the mid height on the
294 tension side. Slight rupture of the one layer CFRP around the mid height of the compression side
295 was observed for Specimens FP-E40, and this slight rupture did not result in the final failure of
296 specimens.
297
298 The test results for specimens under 40 mm eccentric load are presented in Table 3. It can be
299 seen that Specimens P60-E40 carried lowest peak axial loads. Specimens F-E40 achieved the
300 greatest peak axial loads, which were on average 27% higher than the peak axial loads carried by
301 Specimens P60-E40. Specimens FP-E40 achieved peak loads which were on average 26%
302 greater than the average peak axial loads of Specimens P60-E40. Specimens P30-E40 carried
303 peak axial loads that were only on average 5% higher than Specimens P60-E40. Fig. 11 shows
304 the axial load-axial deformation behavior of Specimens F-E40, FP-E40, P30-E40, and P60-E40.
305 All specimens presented post-peak descending branches, which suggests the effectiveness of
306 FRP wrapping in terms of providing a strength increase was insignificant for specimens with
307 large load eccentricity. Even though the peak axial loads for Specimens P30-E40 were only

slightly higher than the peak axial loads of Specimens P60-E40, the deformation capacity, especially the lateral deflection capacities of Specimens P30-E40 were significantly higher than those of Specimens P60-E40.

Influence of Axial Load Eccentricity

The influence of axial load eccentricity on the increase of peak axial loads of different groups of specimens is shown in Fig. 12. In Fig. 12, the vertical axis is $P_2 / (f_{co} \cdot A_g)$ and the horizontal axis is e / d (Note: A_g is the gross cross section area, and d is the diameter of the confined concrete). In general, an increase in the axial load eccentricity led to a significant decrease in the peak axial loads of all specimens. At low axial load eccentricity (e / d =0.1), specimens of Groups P30 and P60 experienced a greater decrease (44% and 45%, respectively) in the peak axial loads than the decrease in the peak axial loads in specimens of Groups F and FP (33% and 36%, respectively). However, as the axial load eccentricity increased, the percentage of decrease in the peak axial loads for different groups of specimens was close. Referring to the specimens tested in Groups F, FP and P30, an overall decrease in peak axial loads of 79.4%, 77.4% and 80.5% was observed when the e / d ratio was increased from 0 to 0.27. Similarly, specimens in Group P60 experienced an overall load decrease of 72.7% in the peak axial loads for the same increment in eccentricity. Moreover, it can be observed that as the axial load eccentricity increased, the difference in peak axial loads for specimens in each group decreased. When specimens were subjected to an eccentric axial load with an e / d ratio of 0.27, the peak axial loads carried by specimens in each group were quite close.

It is noted that the tested specimens were not reinforced with steel bars. Hence, the influence of the longitudinal steel reinforcement on the behavior of FRP confined concrete with different wrapping schemes was not reflected in the test results. Also, the size of the tested specimens was relatively small compared to the full-scale columns. Although the size effect on FRP confined concrete was found insignificant in several previous studies (Carey and Harries 2005; Elsanadedy et al. 2012; Thériault et al. 2004), Jamatia and Deb (2017) reported the existence of size effect on the behavior of FRP confined concrete under axial compression. Hence, the experimental results presented in this study should be translated with caution for large FRP confined reinforced concrete columns.

Ductility Capacity

Ductility is defined as the ability of structural members to deform plastically without substantial loss of strength. For steel reinforced concrete (RC) column, the ductility is usually calculated as the ratio of the axial deformation at 85% post-peak load divided by the axial deformation at the elastic limit (Pessiki and Pieroni 1997):

$$\mu = \frac{\Delta_3}{\Delta_1} \tag{1}$$

where μ is the ductility, Δ_3 is the axial deformation at 85% post-peak load, and Δ_1 is the corresponding axial deformation of the axial load at the elastic limit P_1.

The above definition of ductility is usually not applicable for FRP confined concrete. For sufficiently FRP confined concrete (Fig. 4 (c)) with strain hardening response, the specimens failed at the peak axial load due to FRP rupture. In this case, it is not reasonable to use the axial deformation at 85% post-peak axial load to calculate the ductility. Another case is that for

350 insufficiently FRP confined concrete with strain softening response, the axial load at FRP rupture
351 may be between the peak axial load and 85% post-peak axial load (Fig. 4 (a)). The last case is
352 that the axial load at FRP rupture is lower than 85% post-peak axial load (Fig. 4 (b)). In different
353 cases, the definition of ductility should be selected differently to accurately represent the
354 deformation capacity of specimens.

355 The ductility capacity of all specimens is summarized in Tables 2 and 3. It can be seen that
356 Group F specimens obtained higher ductility compared to the other groups of specimens under
357 both concentric and eccentric axial loads. Even though the average peak axial loads of
358 Specimens P60-E0 were only 49.3% of those of Specimens F-E0, the ductility capacities were
359 almost equal. This again indicates that significant strain localization occurred within the non-
360 wrapped region for partially FRP wrapped concrete. Moreover, with the increase of axial load
361 eccentricities, the ductility capacities for all groups of specimens decreased. When the applied
362 axial load changes from concentric axial load to eccentric axial loads of 15 mm, 25 mm and
363 40mm eccentricities, the decrease of ductility for Group F specimens was 34.2%, 40.8%, and
364 53.3%, respectively. Similar ductility decrease was obtained for Group FP specimens. However,
365 the corresponding decreases in ductility were 54.7%, 73.7%, and 83.7%, respectively, for Group
366 P60 specimens. This indicates that the adverse influence of axial load eccentricity on the
367 ductility of partially FRP wrapped concrete was more severe than those of fully and non-
368 uniformly FRP wrapped concrete.

369

370 **Theoretical Analysis**

371 ***Compressive Strength Prediction for Concentrically Loaded Specimens***

372 The compressive strength of the concentrically loaded specimens was predicted by using a
373 strength model proposed in this study. The Lam and Teng (2003a) model was selected as the
374 base model because it is one of the most widely accepted models for the predictions of the
375 compressive strength of circular FRP confined concrete, which was highlighted by its
376 implementation into ACI 440.2R-08 (ACI 2008). Although the Lam and Teng (2003a) model has
377 been proven to accurately predict the compressive strength of fully FRP wrapped concrete, the
378 model is not able to account for partial or non-uniform wrapping schemes. In order to account
379 for the reduced confinement effectiveness due to partial wrapping, a confinement effectiveness
380 coefficient k_f is introduced into the Lam and Teng (2003a) model. The following expression
381 was developed for compressive strength prediction of fully and partially FRP wrapped concrete:

$$\frac{f_{cc}}{f_{co}} = 1 + 3.3k_f \frac{f_{l,a}}{f_{co}} \tag{2}$$

382 where f_{cc} is the compressive strength of confined concrete; f_{co} is the unconfined compressive
383 strength of concrete; k_f is the confinement effectiveness coefficient; and $f_{l,a}$ is the actual lateral
384 confining pressure.

385 The confinement effectiveness coefficient can be expressed as (Mander et al. 1988; Barros and
386 Ferreira 2008; Pham et al. 2015):

$$k_f = \left(1 - \frac{s}{2d}\right)^2 \tag{3}$$

387 where s is the clear spacing between two adjacent FRP strips and d is the diameter of confined
388 concrete.

389 The actual lateral confining pressure can be taken according to Equation (4), which was
390 proposed for full and partial FRP wrapping schemes in Barros and Ferreira (2008) and Pham et
391 al. (2015):

$$f_{l,a} = \frac{2E_f t_f \varepsilon_{h,rup}}{d} \frac{w}{w+s} \tag{4}$$

392 where E_f is the elastic modulus of FRP; t_f is the thickness of FRP; $\varepsilon_{h,rup}$ is the actual hoop
393 rupture strain of FRP; and w is the width of FRP strips.

394 Using Equations (2), (3) and (4), the compressive strength of concentrically loaded fully and
395 partially FRP wrapped concrete can be predicted. However, further modification was required
396 for specimens with non-uniform wrapping scheme. The non-uniform FRP wrapping was
397 considered to comprise two components, namely, full FRP wrapping and partial FRP wrapping.
398 The confinement provided by the partial FRP wrapping was added to the confinement provided
399 by the full FRP wrapping using the principle of superposition. Therefore, the expression for the
400 compressive strength of concentrically loaded non-uniformly FRP wrapped concrete is as
401 follows:

$$\frac{f_{cc}}{f_{co}} = 1 + 3.3 \frac{f_{lf} + k_f f_{lp}}{f_{co}} \tag{5}$$

402 where f_{lf} is the confining pressure provided by the full FRP wrapping; k_f is the confinement
403 effectiveness coefficient, which can be expressed as $(1 - s/2d)^2$; and f_{lp} is the confining
404 pressure provided by the partial FRP wrapping.

405

406 Strain gauges were attached at the mid-height of the specimen to obtain axial and hoop strains.
407 However, most of the readings of the strain gauges experienced a large scatter due to the poor
408 welding of the wires. Therefore, the recorded strain values were considered not accurate and
409 hence not used. Based on the findings from several studies (Chen et al. 2013; Lam and Teng
410 2003a; Wu and Jiang 2013), the ACI 440.2R-08 (2008) suggests that the strain efficiency factor
411 to be taken as 0.55. Hence, the actual hoop rupture strain was taken as 55% of the nominal
412 tensile strain of FRP. Considering this strain efficiency factor and a nominal FRP rupture strain
413 of 1.7%, the actual FRP hoop rupture strain was determined to be 0.935%. Equations (2) and (5)
414 were applied to predict the compressive strength of all concentrically loaded specimens in this
415 study. Table 4 compares the experimental and analytical results of all concentrically loaded
416 specimens. It is evident that the proposed equations underestimate the compressive strength of
417 Specimens F-E0, FP-0, and P30-E0, with a maximum error of 17% for Specimens F-E0.
418 However, overestimation was obtained for Specimens P60-E0-2 with a maximum error of 23%.
419 The differences between experimental and analytical results indicate that, with the increase of
420 FRP strip spacing, the strength reduction was more significant than the analytical predictions. In
421 general, the proposed equations can provide reasonable predictions for the compressive strengths
422 of the concentrically loaded specimens.
423
424 ***Analytical Interaction (P-M) Diagram***
425 Interaction (*P-M*) diagrams were constructed to investigate the axial load and bending moment
426 capacity of the specimens. For eccentrically loaded specimens, the bending moment capacity
427 considering the second order moment was calculated by Equations (6):

$$M_1 = P_u(e + \delta) \quad (6)$$

where P_u indicates ultimate load, e indicates load eccentricity, and δ indicates lateral deflection at the ultimate load.

The experimental non-dimensional interaction diagrams are shown in Fig. 13. In Fig. 13, the vertical axis is $P_2 / f_{co} \cdot A_g$ and the horizontal axis is $M_1 / f_{co} \cdot A_g \cdot d$, where A_g is the gross cross section area, and d is the diameter of the confined concrete. Group F specimens outperformed the other groups of specimens, followed by Groups FP, P30, and P60 specimens. Moreover, with the increase of eccentricity from 25 mm to 40 mm, the differences between the different groups of specimens became less significant, which indicates that the confinement efficiency was less with the increase of eccentricity. It can also be observed that for an eccentricity of 40 mm, the performance of Groups F and FP specimens was comparable and the performance of Groups P30 and P60 was comparable.

In this section, a numerical fiber element method was used to construct the analytical interaction diagrams of concrete specimens (Fam et al. 2003; Yazici and Hadi 2009; Wang et al. 2016). The cross section of concrete specimens was divided into a finite number of small horizontal strips, as shown in Fig. 14. In each layer, the area of concrete core was calculated. With the plain section assumption, the axial strain in each strip was estimated and the axial stress of each component was calculated by the stress-strain model of concrete. The calculated stresses were then integrated over the whole cross section area to obtain the resultant force and the resultant moment. For a given eccentricity e, the depth of neutral axis, d_n, was first assumed. Based on the assumed neutral axis and the ultimate axial strain at the extreme compression fiber of the section, the resultant force and the resultant bending moment were obtained. Afterwards, the

eccentricity e' was obtained by dividing the bending moment by the force. If the calculated eccentricity e' was the same with the given eccentricity e, the calculation was completed and the calculated force and bending moment were the true values. If not, the depth of neutral axis was readjusted. The above procedure was repeated until the calculated eccentricity e' was the same with the given eccentricity e. In order to get more accurate prediction results, the width of the strips should be small enough. In this study, the width of the strips was taken as 1 mm. For FRP materials, a linear elastic stress-strain relationship was adopted. The tensile stress carried by the concrete was neglected in this study. For concrete under compression, the stress-strain model proposed by Lam and Teng (2003a) was adopted for the FRP confined concrete subjected to concentric axial load, which can be described by the following expressions:

$$\sigma_c = E_c \varepsilon_c - \frac{(E_c - E_2)^2}{4 f_{co}} \varepsilon_c^2 \text{ for } 0 \le \varepsilon_c \le \varepsilon_t \tag{7}$$

$$\sigma_c = f_{co} + E_2 \varepsilon_c \qquad \text{for } \varepsilon_t \le \varepsilon_c \le \varepsilon_{cu} \tag{8}$$

where σ_c and ε_c are the axial stress and axial strain, respectively; E_c is the elastic modulus of unconfined concrete; E_2 is the slope of the linear second portion of the stress-strain curve; and ε_{cu} is the ultimate axial strain of confined concrete. The parabolic first portion meets the linear second portion with a smooth transition at ε_t:

$$\varepsilon_t = \frac{2 f_{co}}{(E_c - E_2)} \tag{9}$$

The slope of the linear second portion E_2 is given by

$$E_2 = \frac{f_{cc} - f_{co}}{\varepsilon_{cu}} \tag{10}$$

where f_{cc} is the compressive strength of confined concrete. In this study, the compressive strengths of Groups F, P30, and P60 specimens subjected to concentric axial load were predicted by Equation (2), while the compressive strength of Group FP specimens subjected to concentric axial load were predicted by Equation (5). The ultimate axial strain ε_{cu} can be calculated by (Lam and Teng 2003):

$$\frac{\varepsilon_{cu}}{\varepsilon_{co}} = 1.75 + 12\left(\frac{f_{l,a}}{f_{co}}\right)\left(\frac{\varepsilon_{h,rup}}{\varepsilon_{co}}\right)^{0.45} \tag{11}$$

where ε_{co} is the compressive strain of concrete corresponding to f_{co}.

Moreover, in order to consider the reduced effectiveness of FRP confinement for concrete core subjected to eccentric load, a variable confinement model was adopted to describe the stress-strain relationship of concrete core under eccentric axial load (Yu et al. 2010). This model is an extension of Teng et al. (2009) model. The only difference is the value of the slope of the second linear portion of the concrete stress-strain curve E_2. For concrete under eccentric axial load, the slope of the second linear portion of the stress-strain curve was calculated as:

$$E_{2ec} = E_2 \frac{d}{d+e} \tag{12}$$

where E_{2ec} is the slope of the second linear portion of the concrete stress-strain curve, and d is the diameter of confined concrete.

480 It should be noted that the above concrete stress-strain model is only suitable for sufficiently
481 FRP confined concrete with strain hardening response (Bisby and Ranger 2010). For
482 insufficiently FRP wrapped concrete as well as for specimens failed due to concrete cracking, the
483 above concrete stress-strain curve reduces to a stress-strain curve composed of an initial parabola
484 followed by a horizontal straight line (ACI 440.2R 2008; Lam and Teng 2003a; Rocca et al.
485 2009). The compressive strength equals to the unconfined concrete strength, and the ultimate
486 axial strain was assumed to be 0.003, as suggested in ACI 440.2R (2008). Fig. 15 compares the
487 experimental and analytical interaction diagrams (non-dimensional) of different groups of
488 specimens. For comparison purpose, the bending moment capacity without considering the
489 second order moment was also calculated and presented in Fig. 15:

$$M_2 = P_2 \cdot e \tag{13}$$

490 For Groups F and FP specimens, the analytical interaction diagrams were significantly lower
491 than the experimental P-M_1 interaction diagrams. The difference between the experimental and
492 analytical compressive strength was relatively small (as shown in Table 4), while the analytical
493 bending moment was much lower than the experimental bending moment M_1. For Group P30
494 specimens, the analytical interaction diagrams were lower than the experimental P-M_1 interaction
495 diagrams, but the difference was not significant. While for Group P60 specimens, the analytical
496 results were significantly higher than the experimental P-M_1 interaction diagrams. In general, by
497 using the proposed fiber element method, conservative predictions can be obtained for Groups F,
498 FP, and P30 specimens, which is safe for the column design. This conclusion was similar to the
499 observations reported in Bisby and Ranger (2010). Nevertheless, the analytical results were
500 significantly higher than the experimental P-M_1 interaction diagrams for Group P60 specimens.
501 This may be because the non-wrapped concrete began to spall off after the unconfined

compressive strength was reached, which may result in the performance deterioration of specimens. However, the spalling of non-wrapped concrete (i.e., loss of cross sectional area) was not taken into consideration by the proposed analytical method. With the increase of the spacing of FRP strips, the spalling of non-wrapped concrete became more severe and thus greater error between experimental and analytical results was observed. Therefore, a more accurate analytical model needs to be developed for partially FRP wrapped concrete to account for the performance deterioration of specimens due to spalling of non-wrapped concrete.

Conclusions

Experimental and analytical studies were carried out to investigate the performance of fully, partially, and non-uniformly FRP wrapped concrete under concentric and eccentric axial loads. The following conclusions can be drawn:

1. The axial load carrying capacity of fully FRP wrapped concrete is the highest under both concentric and eccentric axial loads, followed by non-uniformly and partially FRP wrapped concrete. Moreover, the peak axial load of the specimen is significantly reduced with the increase in the axial load eccentricity for all groups of specimens.

2. The failure mode of the specimen is influenced by the axial load eccentricity. The FRP rupture is the main failure mode for specimens tested at lower axial load eccentricities, whereas concrete tension cracking failure is the dominate failure mode for specimens tested at higher axial load eccentricities. The transfer from FRP rupture failure to concrete tension cracking failure occurs at lower axial load eccentricities for partially wrapped specimens than for the fully and non-uniformly wrapped specimens.

3. Equations are proposed to predict the compressive strength of FRP wrapped concrete with different wrapping schemes. As for non-uniformly FRP wrapped concrete, the confinement is composed of two components, namely, confinement provided by full FRP wrapping and confinement provided by partial FRP wrapping. By using the principle of superposition, the compressive strength can be predicted with a reasonable accuracy.

4. Experimental and analytical interaction diagrams are constructed to investigate the behavior of eccentrically loaded specimens. In general, the analytical model reasonably predicts the compressive strengths of Groups F and FP specimens, but underestimates the bending moment capacities. The analytical model overestimates the compressive strengths of Groups P30 and P60 specimens. With the increase of the spacing of FRP strips gaps, the overestimation of bending moment become more significant for partially FRP wrapped concrete. These overestimations occur mainly because the analytical model does not consider the performance deterioration of partially FRP wrapped concrete, which is due to the spalling of non-wrapped concrete.

5. Non-uniform wrapping combines the advantages of full and partial wrapping. Compared to partial wrapping, the non-uniform wrapping provides higher strength and ductility under both concentric and eccentric axial loads. Moreover, for partially FRP wrapped concrete, the non-wrapped concrete may be exposed to harsh environment (e.g., moisture, heat, and impact), which may deteriorate the performance of concrete (e.g., corrosion of inner steel reinforcement and concrete spalling). By wrapping FRP non-uniformly, these adverse effects can be alleviated. Meanwhile, after fewer layers of full wrapping, the remaining layers of partial wrapping can only be applied onto the deteriorated parts of the columns. Therefore, the consumption of FRP may be less than in the case of full wrapping.

546

547

548 **Acknowledgments**

549 The authors gratefully acknowledge the contributions of Mr. Ritchie Mclean for his help in
550 carrying out the experiments.

551

552 **References**

553 ACI 440.2R-08. (2008). "Guide for the design and construction of externally bonded FRP
554 systems for strengthening concrete structures." ACI 440.2R-08, American Concrete Institute,
555 Detroit.

556 ASTM. (2010). “Standard test method for tensile properties of fiber reinforced polymer matrix
557 composites used for strengthening of civil structures.” D7565, West Conshohocken, PA.

558 Barros, J., and Ferreira, D. (2008). “Assessing the efficiency of CFRP discrete confinement
559 systems for concrete cylinders.” Journal of Composites for Construction, 12(2), 134-148.

560 Bestech Australia Pty Ltd. (2018). “Laser Triangulation”. ⟨http://www.bestech.com.au/laser-
561 triangulation-sensor/⟩ (Accessed on Jan. 4, 2018).

562 Campione, G., La Mendola, L., Monaco, A., Valenza, A., and Fiore, V. (2015). “Behavior in
563 compression of concrete cylinders externally wrapped with basalt fibers.” Composites Part B:
564 Engineering, 69(0), 576-586.

565 Carey, S. A., and Harries, K. A. (2005). “Axial behavior and modeling of confined small-,
566 medium- and large scale circular sections with carbon fiber-reinforced polymer jackets.” ACI
567 Structural Journal, 102(4), 596–604.

568 Chen, J., Li, S., and Bisby, L. (2013). "Factors Affecting the Ultimate Condition of FRP-
569 Wrapped Concrete Columns." J. Compos. Constr., 10.1061/(ASCE)CC.1943-5614.0000314, 67-
570 78.

571 Elsanadedy, H. M., Al-Salloum, Y. A., Alsayed, S. H., and Iqbal, R. A. (2012). "Experimental
572 and numerical investigation of size effects in FRP-wrapped concrete columns." Construction and
573 Building Materials, 29, 56-72.

574 Hadi, M. N. S. (2006a). “Behaviour of FRP wrapped normal strength concrete columns under
575 eccentric loading.” Composite Structures, 72(4), 503–511.

576 Hadi, M. N. S. (2006b). “Comparative study of eccentrically loaded FRP wrapped columns.”
577 Composite Structures, 74(2), 127–135.

578 Hadi, M. N. S., Wang, W., and Sheikh, M. N. (2015). “Axial compressive behavior of GFRP
579 tube reinforced concrete columns.” Construction and Building Materials, 81, 198–207.

580 Jamatia, R., and Deb, A. (2017). "Size Effect in FRP-Confined Concrete under Axial
581 Compression." Journal of Composites for Construction, 21(6), 04017045.

582 Lam, L., and Teng, J. G. (2003a). “Design-oriented stress-strain model for FRP-confined
583 concrete.” Construction and Building Materials, 17(6–7), 471–489.

584 Lam, L., and Teng, J. G. (2003b). “Design-oriented stress-strain model for FRP-confined
585 concrete in rectangular columns.” Journal of Reinforced Plastics and Composites, 22(13), 1149-
586 1186.

587 Mander, J. B., Priestley, M. J., and Park, R. (1988). "Theoretical stress-strain model for confined
588 concrete." Journal of Structural Engineering (United States), 114(8), 1804-1826.

589 Matthys, S., Toutanji, H., Audenaert, K., and Taerwe, L. (2005). “Axial load behavior of large-
590 scale columns confined with fiber-reinforced polymer composites.” ACI Structural Journal,
591 102(2), 258-267.

592 Nanjing Hitech Composites Co.,Ltd. (2016). “CFRP”. ‧http://www.hitechfrp.com/goods-show-
593 919.htm‧ (Jun. 1, 2016).

594 Park, T. W., Na, U. J., Chung, L., and Feng, M. Q. (2008). “Compressive behavior of concrete
595 cylinders confined by narrow strips of CFRP with spacing.” Composites Part B: Engineering,
596 39(7-8), 1093-1103.

597 Parvin, A. and Wang, W. (2001). "Behavior of FRP jacketed concrete columns under eccentric
598 loading." Journal of Composites for Construction, 5(3), 146-152.

599 Pessiki, S., and Pieroni, A. (1997). “Axial load behavior of large-scale spirally-reinforced high-
600 strength concrete columns.” ACI Structural Journal, 94(3), 304-314.

601 Pham, T. M., Hadi, M. N. S., and Youssef, J. (2015). “Optimized FRP wrapping schemes for
602 circular concrete columns under axial compression.” Journal of Composites for Construction,
603 19(6).

604 Rocca, S., Galati, N., and Nanni, A. (2009). "Interaction diagram methodology for design of
605 FRP-confined reinforced concrete columns." Construction and Building Materials, 23(4), 1508-
606 1520.

607 Rousakis, T. C. (2014). "Elastic fiber ropes of ultrahigh-extension capacity in strengthening of
608 concrete through confinement." Journal of Materials in Civil Engineering, 26(1), 34-44.

609 Rousakis, T. C. (2016). "Reusable and recyclable nonbonded composite tapes and ropes for
610 concrete columns confinement." Composites Part B: Engineering, 103, 15-22.

611 Saadatmanesh, H., Ehsani, M. R., and Li, M. W. (1994). "Strength and ductility of concrete
612 columns externally reinforced with fiber composite straps." ACI Structural Journal, 91(4), 434-
613 447.

614 Saljoughian, A., and Mostofinejad, D. (2016). "Axial-flexural interaction in square RC columns
615 confined by intermittent CFRP wraps." Composites Part B: Engineering, 89, 85-95.

616 Thériault, M., Neale, K. W., and Claude, S. (2004). "Fiber-Reinforced Polymer-Confined
617 Circular Concrete Columns: Investigation of Size and Slenderness Effects." Journal of
618 Composites for Construction, 8(4), 323-331.

619 Triantafyllou, G. G., Rousakis, T. C., and Karabinis, A. I. (2015). "Axially loaded reinforced
620 concrete columns with a square section partially confined by light GFRP straps." Journal of
621 Composites for Construction, 19(1).

622 Wei, H., Wu, Z., Guo, X., and Yi, F. (2009). "Experimental study on partially deteriorated
623 strength concrete columns confined with CFRP." Engineering Structures, 31(10), 2495-2505.

624 Wei, Y., and Wu, Y.-F. (2016). "Experimental Study of Concrete Columns with Localized
625 Failure." Journal of Composites for Construction, 20(5), 04016032.

626 Wu, Y.-F., and Jiang, C. (2013). "Effect of load eccentricity on the stress-strain relationship of
627 FRP-confined concrete columns." Composite Structures, 98, 228–241.

628 Wu, Y.-F., and Jiang, J.-F. (2013). "Effective strain of FRP for confined circular concrete
629 columns." Composite Structures, 95, 479-491.

630 Wang, W., Sheikh, M. N., and Hadi, M. N. S. (2015). "Axial compressive behaviour of concrete
631 confined with polymer grid." Materials and Structures/Materiaux et Constructions, 1-16.

632 Wang, W., Sheikh, M. N., and Hadi, M. (2016). "Experimental study on FRP tube reinforced
633 concrete columns under different loading conditions." Journal of Composites for Construction,
634 10.1061/(ASCE)CC.1943-5614.0000690, 04016034.

635 Wang, W., Sheikh, M. N., Hadi, M. N. S., Gao, D., and Chen, G. (2017). "Behaviour of
636 concrete-encased concrete-filled FRP tube (CCFT) columns under axial compression."
637 Engineering Structures, 147, 256-268.

638 Yazici, V., and Hadi, M. N. S. (2009). "Axial load-bending moment diagrams of carbon FRP
639 wrapped hollow core reinforced concrete columns." Journal of Composites for Construction,
640 13(4), 262-268.

641 Yu, T., Wong, Y. L., and Teng, J. G. (2010). “Behavior of hybrid FRP-concrete-steel double-
642 skin tubular columns subjected to eccentric compression.” Advances in Structural Engineering,
643 13(5), 961-974.

Table 1. Test matrix

Specimen	Wrapping scheme	FRP layers	Strip spacing	Test Mode
F-E0-1,2	Full	2 full layers	0	e=0 mm
F-E15-1,2	Full	2 full layers	0	e=15 mm
F-E25-1,2	Full	2 full layers	0	e=25 mm
F-E40-1,2	Full	2 full layers	0	e=40 mm
P30-E0-1,2	Partial	4 partial layers	30	e=0 mm
P30-E15-1,2	Partial	4 partial layers	30	e=15 mm
P30-E25-1,2	Partial	4 partial layers	30	e=25 mm
P30-E40-1,2	Partial	4 partial layers	30	e=40 mm
P60-E0-1,2	Partial	6 partial layers	60	e=0 mm
P60-E15-1,2	Partial	6 partial layers	60	e=15 mm
P60-E25-1,2	Partial	6 partial layers	60	e=25 mm
P60-E40-1,2	Partial	6 partial layers	60	e=40 mm
FP-E0-1,2	Non-uniform	1 full layer and 2 partial layers	-	e=0 mm
FP-E15-1,2	Non-uniform	1 full layer and 2 partial layers	-	e=15 mm
FP-E25-1,2	Non-uniform	1 full layer and 2 partial layers	-	e=25 mm
FP-E40-1,2	Non-uniform	1 full layer and 2 partial layers	-	e=50 mm

Table 2. Test results of specimens under concentric axial load

Specimen	P_1 (kN)	δ_1 (mm)	P_2 (kN)	δ_2 (mm)	δ_3 (mm)	μ	Failure mode
F-E0-1	771	1.1	1542	9.1	-	8.9	I
F-E0-2	757	1.1	1612	9.7	-		I
FP-E0-1	790	1.3	1450	8.3	-	6.9	I
FP-E0-2	778	1.2	1414	8.5	-		I
P30-E0-1	816	1.4	1375	8.7	-	7.1	I
P30-E0-2	781	1.5	1378	11.8	-		I
P60-E0-1	766	1.3	987	9.7	-	8.1	I
P60-E0-2	760	1.2	893	10.8	-		I
P-E0-1	614	0.9	681	1.2	1.6	1.7	-
P-E0-2	601	0.9	664	1.2	1.5		-

Note: The failure mode “I” indicates FRP rupture failure.

Table 3. Test results of specimens under eccentric axial load

Specimen	P_1 (kN)	Δ_1 (mm)	δ_1 (mm)	P_2 (kN)	Δ_2 (mm)	δ_2 (mm)	Δ_3 (mm)	δ_3 (mm)	μ	Failure mode
F-E15-1	615	1.3	0.1	1053	7.4	8.9	-	-	5.9	I
F-E15-2	596	1.2	0.3	1069	7.5	7.2	-	-		I
FP-E15-1	565	1.3	0.8	872	5.5	2.0	-	-	4.5	I
FP-E15-2	593	1.4	0.5	959	6.9	7.0	-	-		I
P30-E15-1	610	2.7	1.8	751	7.0	8.6	-	-	2.6	I
P30-E15-2	641	3.4	1.6	789	8.3	8.9	-	-		I
P60-E15-1	482	1.2	0.5	517	1.6	0.6	5.7	9.9	3.7	II
P60-E15-2	493	1.8	0.6	529	2.4	1.5	5.1	9.3		II
F-E25-1	499	1.3	0.3	802	7.8	7.9	-	-	5.3	I
F-E25-2	526	1.6	0.7	790	7.3	8.8	-	-		I
FP-E25-1	488	1.2	0.4	697	5.5	5.9	-	-	4.1	I
FP-E25-2	473	1.7	1.1	687	6.1	9.6	-	-		I
P30-E25-1	495	1.2	1.2	576	4.4	8.2	6.7	14.3	3.3	I+II
P30-E25-2	489	1.4	1.0	560	4.1	2.8	7.4	15.8		I+II
P60-E25-1	464	1.1	1.7	493	1.3	1.7	2.3	4.0	2.1	II
P60-E25-2	421	1.2	1.0	441	1.4	1.1	2.8	4.7		II
F-E40-1	282	1.1	1.6	322	2.7	6.7	5.4	10.5	4.6	II
F-E40-2	279	1.2	1.1	328	3.0	4.4	5.5	15.2		II
FP-E40-1	294	1.1	0.7	323	2.5	4.5	4.7	13.2	4.6	II
FP-E40-2	291	1.0	1.0	324	2.3	4.0	4.7	12.3		II
P30-E40-1	246	1.2	0.8	267	1.7	1.5	2.9	5.9	2.1	II
P30-E40-2	252	1.5	0.9	269	1.9	2.0	2.7	4.8		II
P60-E40-1	261	1.0	0.6*	278	1.2	0.9*	1.5	-	1.3	II
P60-E40-2	225	0.8	0.2*	235	0.9	0.3*	1.0	-		II

Note: “I” indicates FRP rupture failure; and “II” indicates concrete tension failure. *Lateral displacement data for S60-E40 specimens affected by crushing and spalling of concrete.

Table 4. Comparisons between Experimental and Analytical Compressive Strength of Specimens

Specimen	Experimental compressive strength (MPa)	Analytical compressive strength (MPa)	Average absolute error (%)
F-E0-1	87.3	77.8	12.2
F-E0-2	91.2		17.2
F-E15-1	59.6	54.9	8.6
F-E15-2	60.5		10.2
F-E25-1	45.4	42.2	7.6
F-E25-2	44.7		5.9
F-E40-1	18.2	16.8	8.3
F-E40-2	18.5		10.1
FP-E0-1	82.0	74.6	9.9
FP-E0-2	80.0		7.2
FP-E15-1	49.3	50.3	2.0
FP-E15-2	54.2		7.7
FP-E25-1	39.4	38.8	1.5
FP-E25-2	38.9		0.2
FP-E40-1	18.3	16.8	8.9
FP-E40-2	18.3		8.9
P30-E0-1	77.8	71.5	8.8
P30-E0-2	78.0		9.1
P30-E15-1	42.5	49.3	13.8
P30-E15-2	44.7		9.3
P30-E25-1	32.6	38.1	14.4
P30-E25-2	31.7		16.8
P30-E40-1	15.1	15.2	0.6
P30-E40-2	15.2		0
P60-E0-1	55.9	65.9	15.2
P60-E0-2	50.5		23.4
P60-E15-1	29.3	38.4	23.7
P60-E15-2	29.9		22.1
P60-E25-1	27.9	30.3	7.9
P60-E25-2	24.9		17.8
P60-E40-1	15.7	15.3	2.6
P60-E40-2	13.3		13.1

Note: The peak strength of concentrically loaded specimens was predicted by the proposed equations, while the peak strength of eccentrically loaded specimens was predicted by the proposed numerical fiber element method.

List of Figures

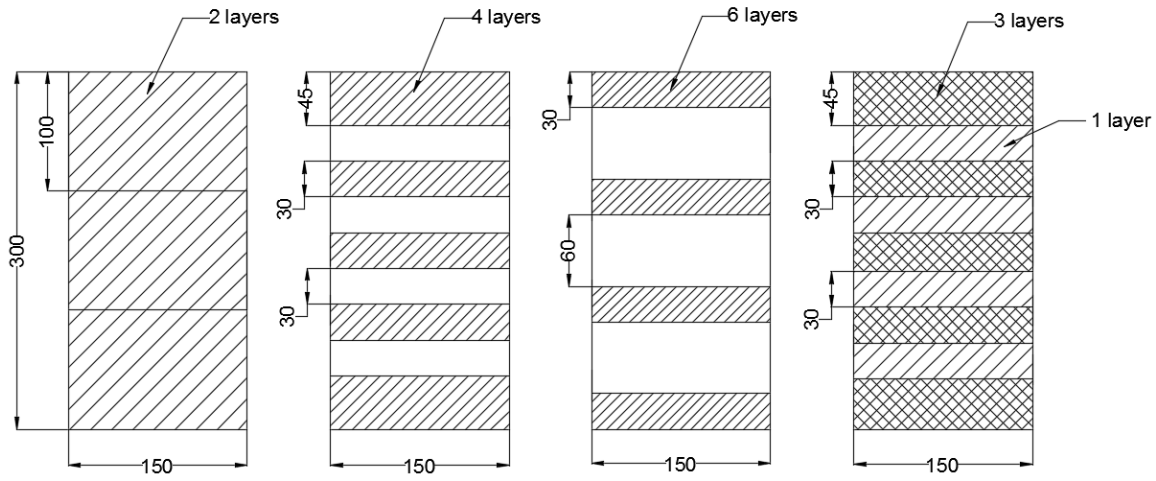

(a) Group F (b) Group P30 (c) Group P60 (d) Group FP

Fig. 1. Details of test specimens (units: mm)

(a) Eccentric loading scheme

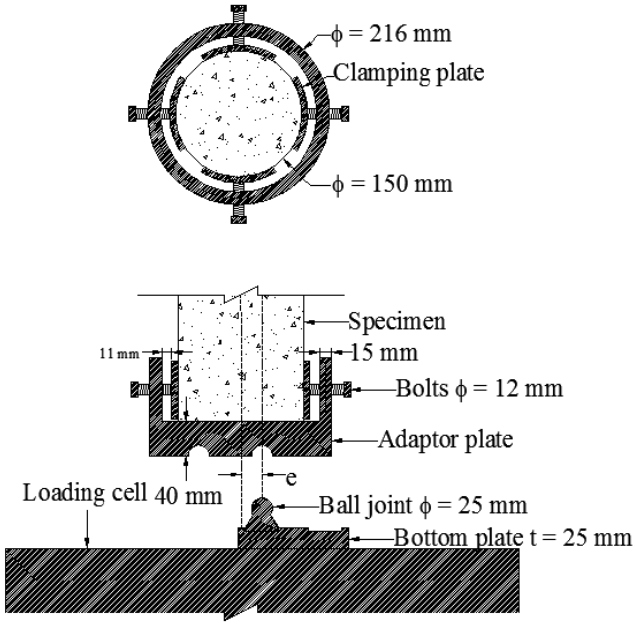

(b) Eccentric loading mechanism

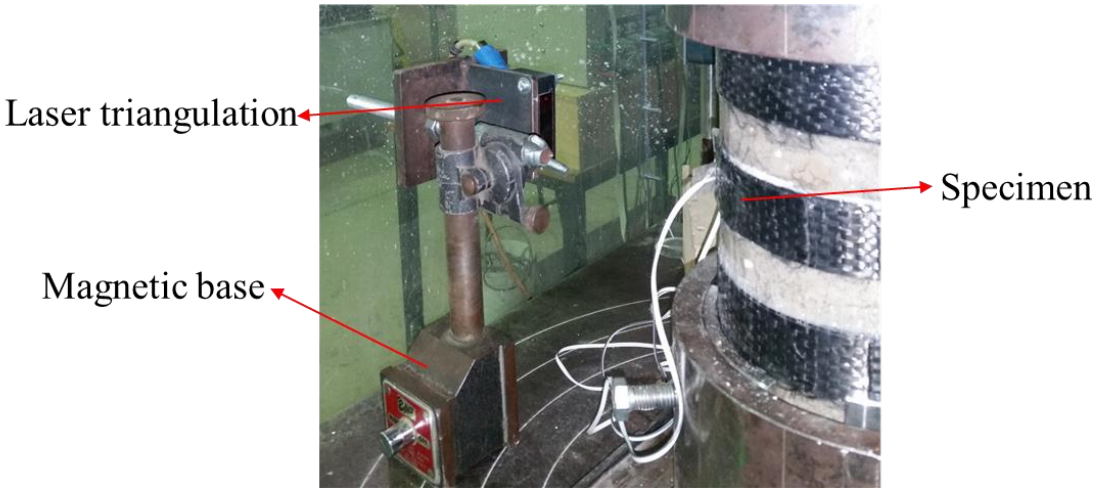

(c) Laser triangulation setup

Fig. 2. Experimental setup

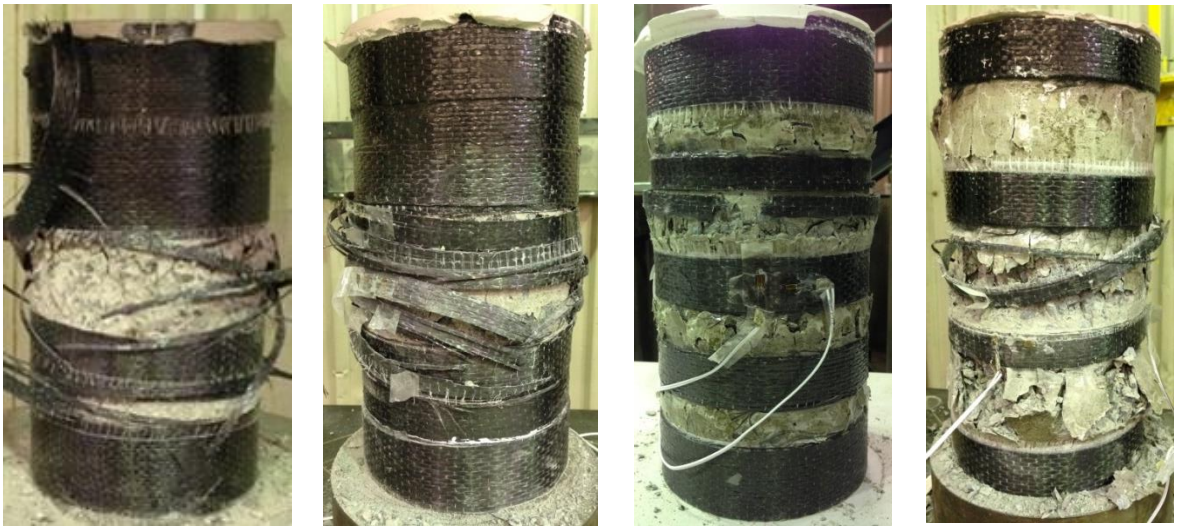

(a) F-E0 (b) FP-E0 (c) P30-E0 (d) P60-E0

Fig. 3. Typical failure modes for specimens under concentric axial load

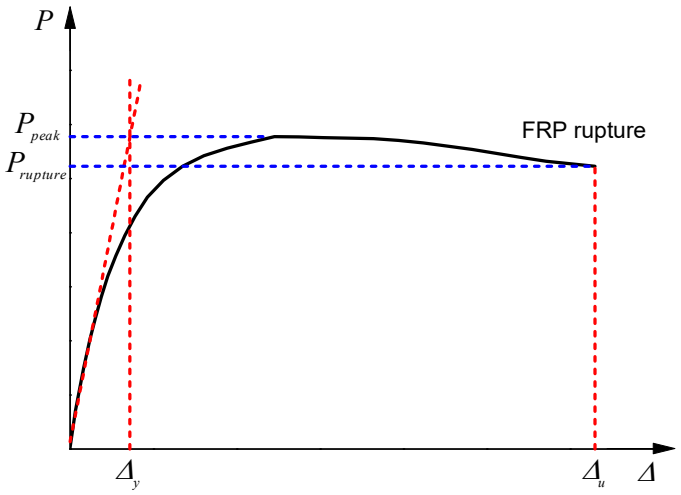

(a) Case 1: Axial load at FRP rupture is between the peak and 85% post-peak axial load

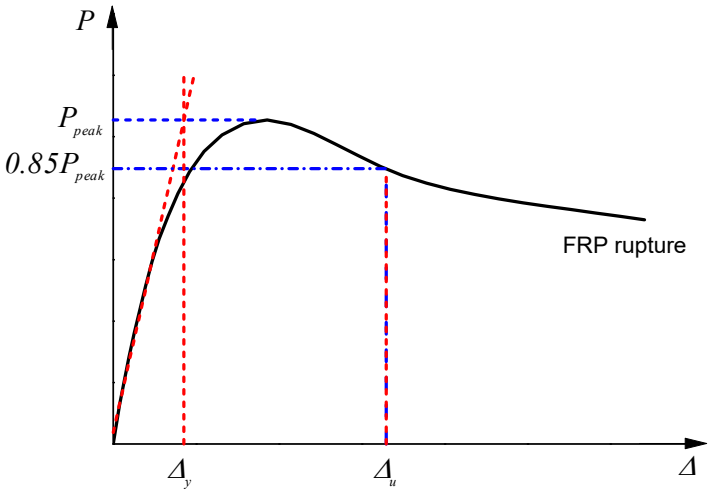

(b) Case 2: Axial load at FRP rupture is below the 85% post-peak axial load

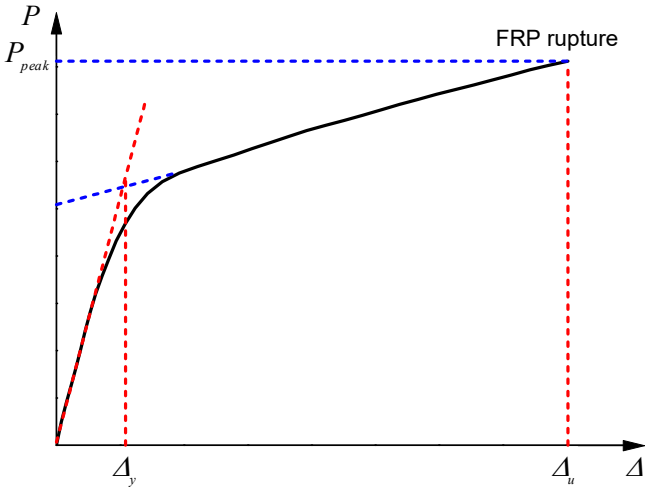

(c) Case 3: Axial load at FRP rupture equals the peak axial load

Fig. 4. Definitions of elastic limit point and ultimate point

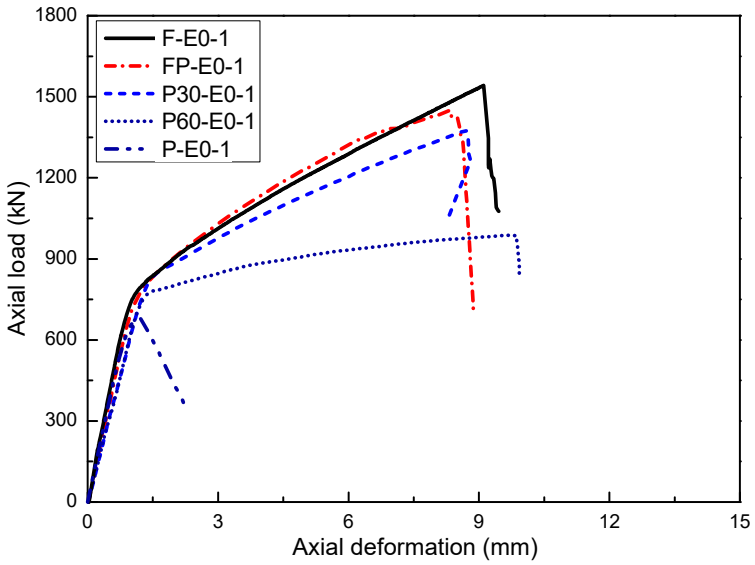

(a) Series A

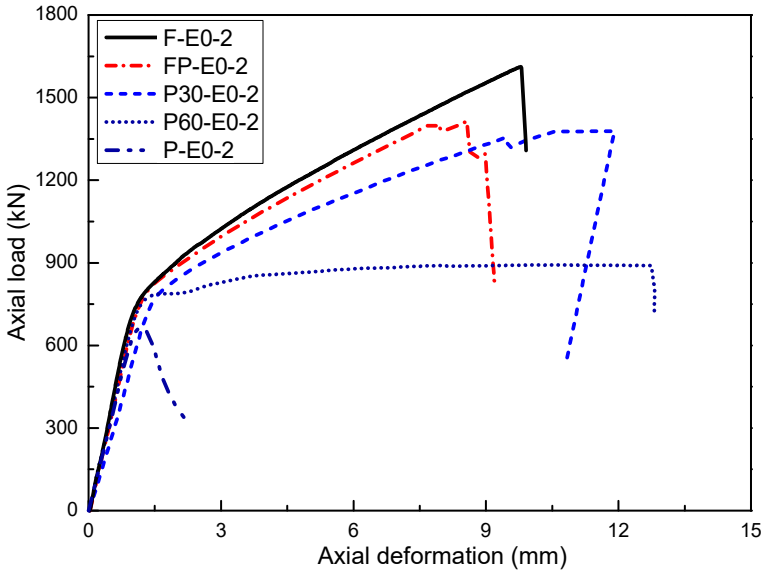

(b) Series B

Fig. 5. Axial load-axial deformation behavior of specimens under concentric axial load

(a) F-E15 (b) FP-E15 (c) P30-E15 (d) P60-E15

Fig. 6. Typical failure modes of specimens under eccentric axial load (e=15 mm)

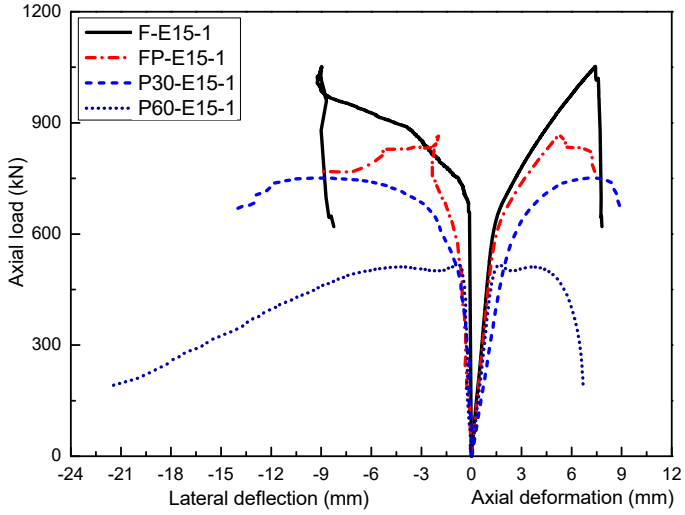

(a) Series A

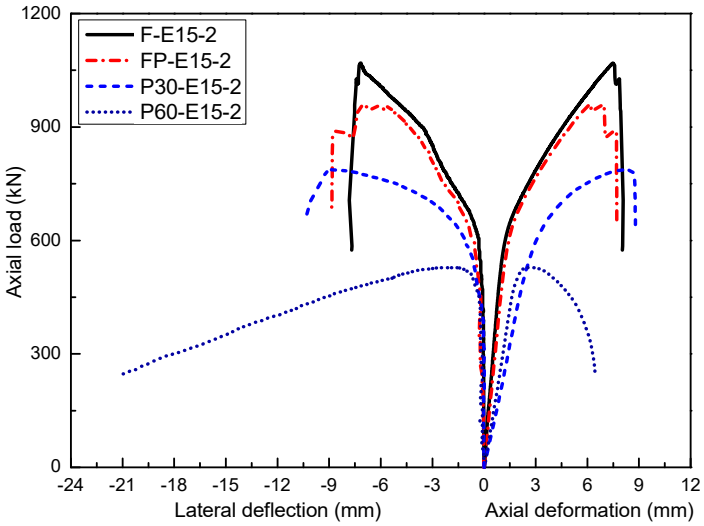

(b) Series B

Fig. 7. Axial load-axial deformation behavior of specimens under eccentric axial load (e=15 mm)

(a) F-E25 (b) FP-E25 (c) P30-E25 (d) P60-E25

Fig. 8. Typical failure modes of specimens under eccentric axial load (e=25 mm)

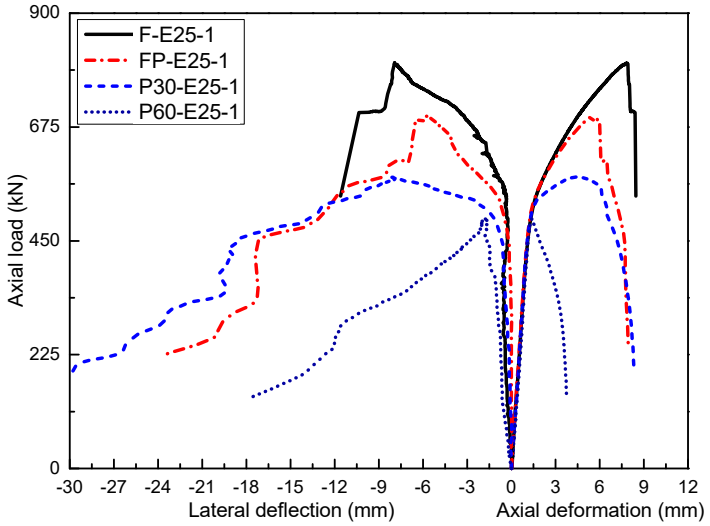

(a) Series A

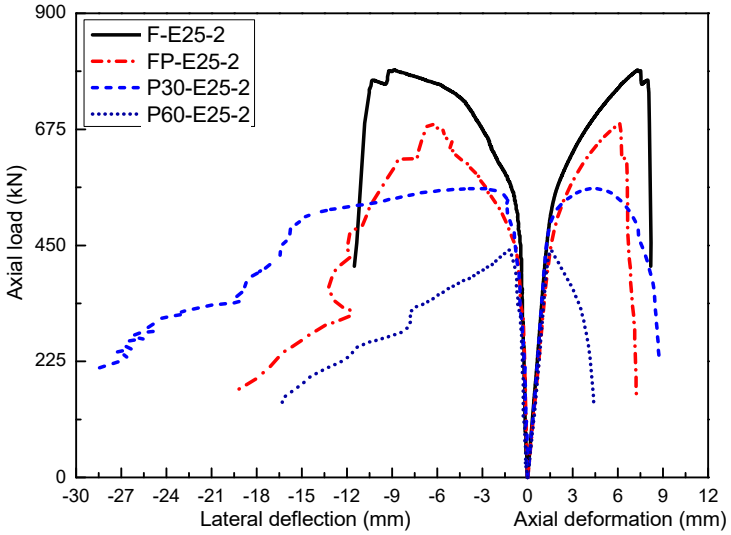

(b) Series B

Fig. 9. Axial load-deformation behavior of specimens under eccentric axial load (e= 25 mm)

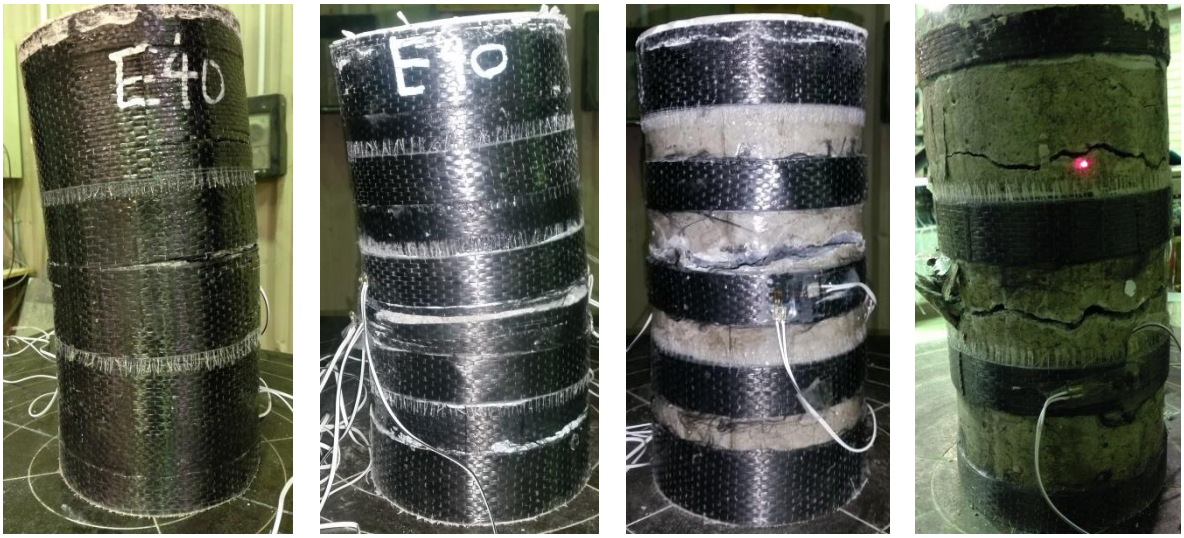

(a) F-E40 (b) FP-E40 (c) P30-E40 (d) P60-E40

Fig. 10. Typical failure modes for specimens under eccentric axial load (e=40 mm)

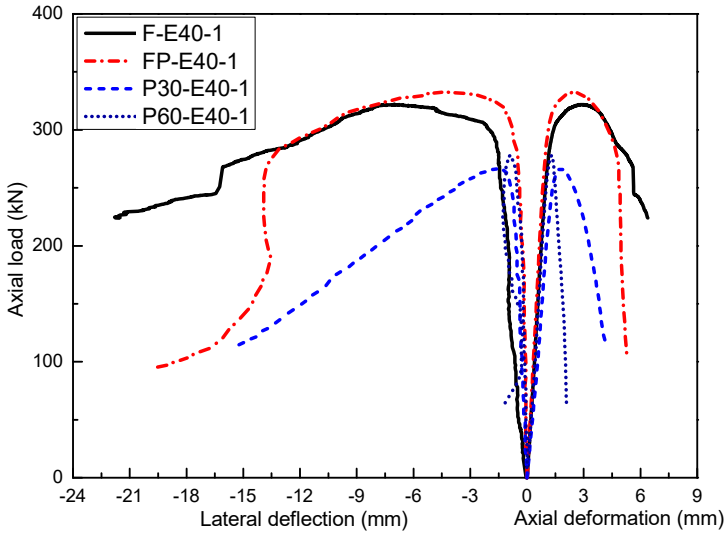

(a) Series A

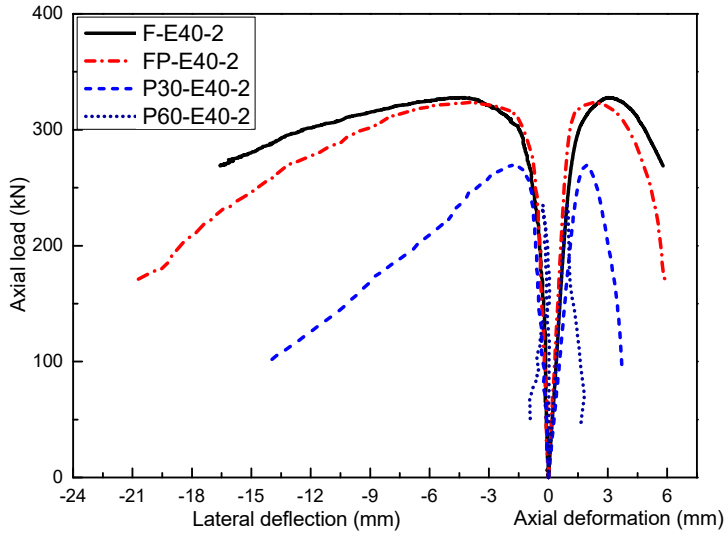

(b) Series B

Fig. 11. Axial load-deformation behavior of specimens under eccentric axial load (e= 40 mm)

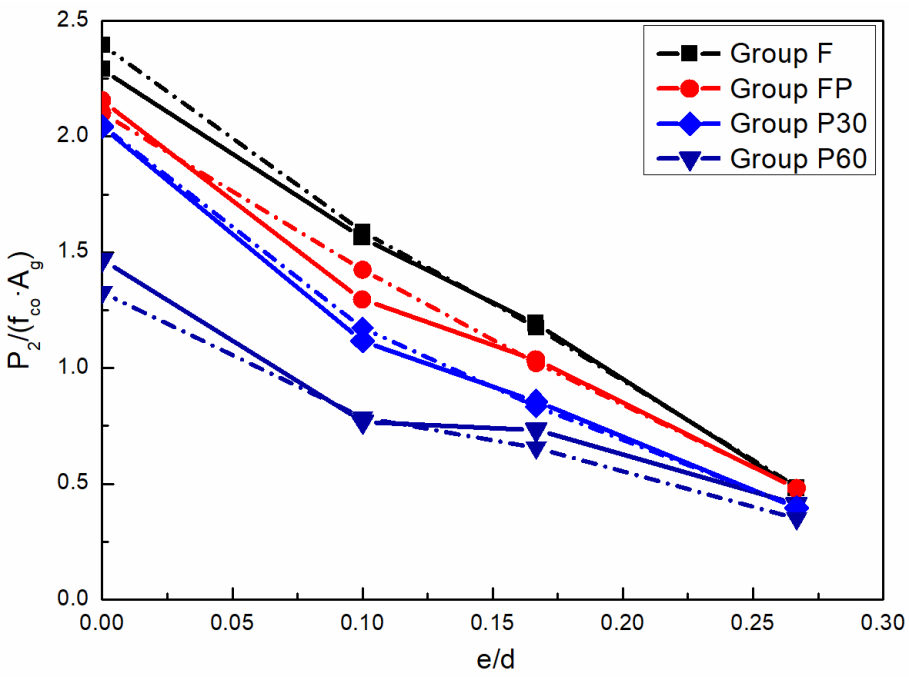

Fig. 12. Influence of axial load eccentricity on the peak axial load

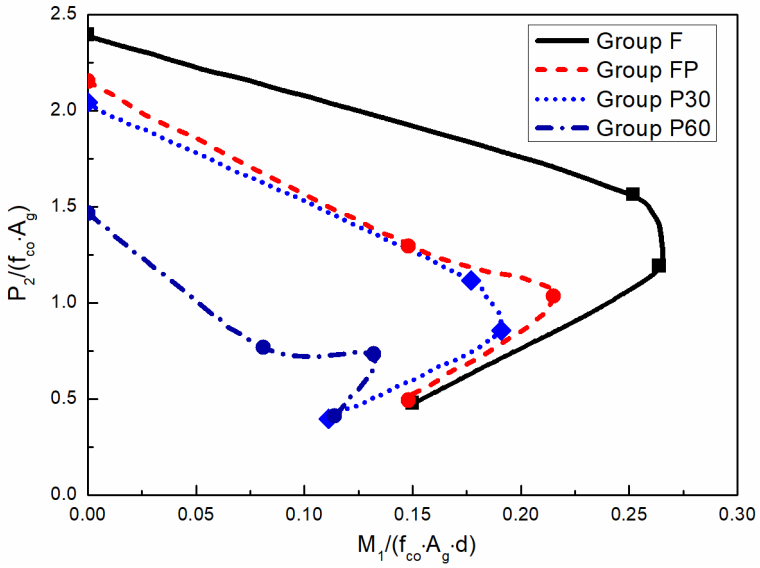

(a) Series A

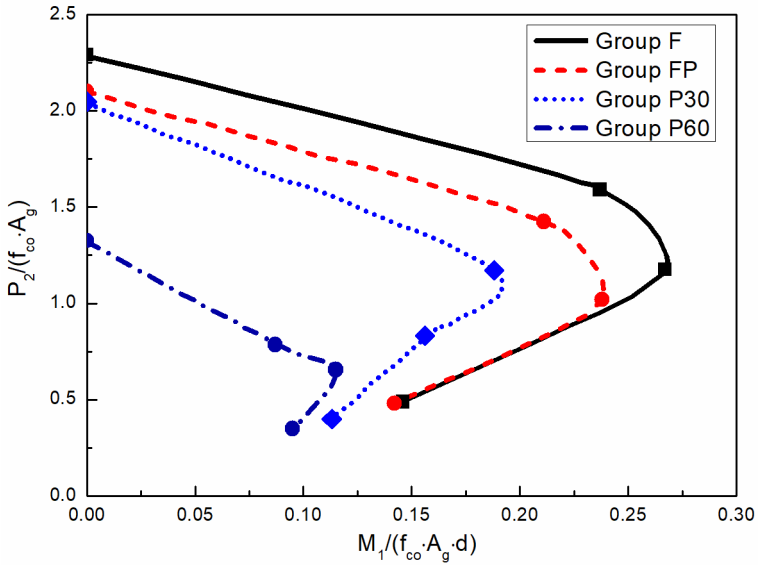

(b) Series B

Fig. 13. Experimental interaction (P − M) diagrams (non-dimensional)

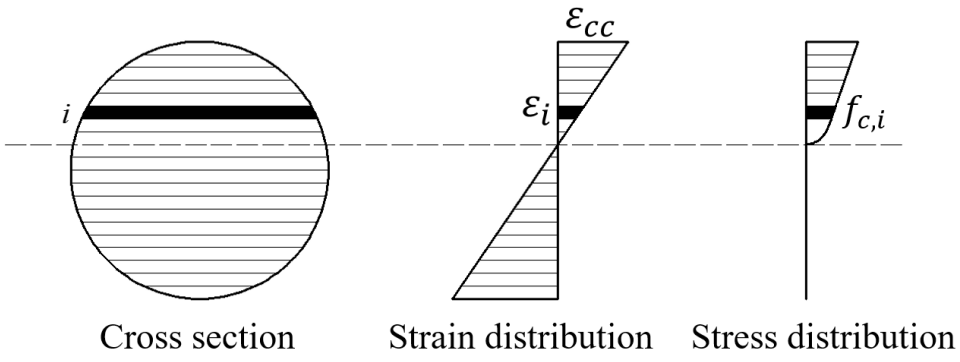

Fig. 14. Strain and stress distributions over the cross section

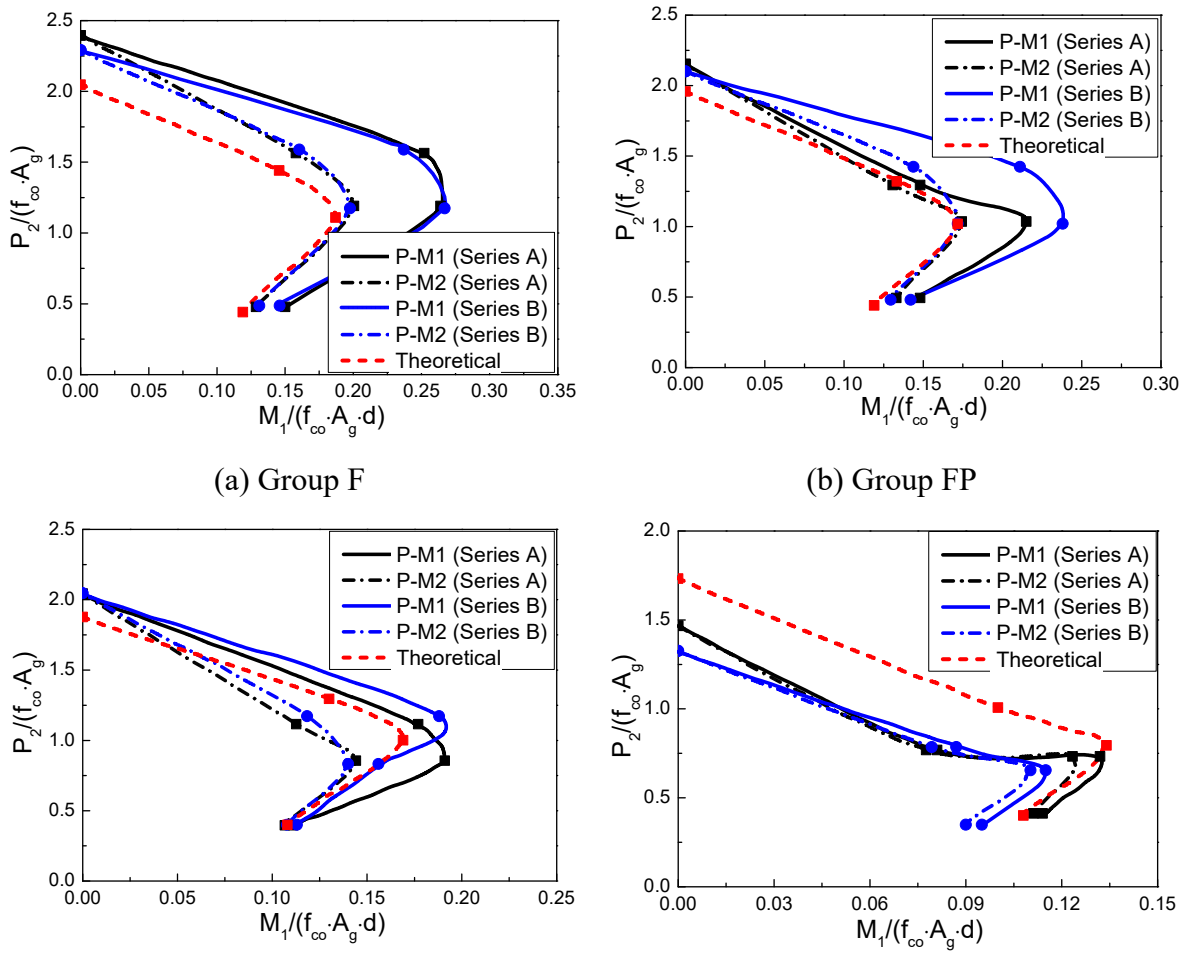

(a) Group F

(b) Group FP

(c) Group P30

(d) Group P60

Fig. 15. Comparison between analytical and experimental interaction (P −M) diagrams (non-dimensional)